# First-principles study of electronic properties of biaxially strained silicon: Effects on charge carrier mobility

Decai Yu,* Yu Zhang, and Feng Liu†
*Department of Materials Science and Engineering, University of Utah, Salt Lake City, Utah 84112, USA*
(Received 22 April 2008; revised manuscript received 16 September 2008; published 16 December 2008)

Using first-principles method, we calculate the electronic band structure of biaxially strained silicon, from which we analyze the change in electron and hole effective mass as a function of strain and determine the mobility of electrons and holes in the biaxially strained silicon based on Boltzmann transport theory. We found that electron mobility increases with tensile strain and decreases with compressive strain. Such changes are mainly caused by a strain-induced change in electron effective mass, while the suppression of intervalley scattering plays a minor role. On the other hand, the hole mobility increases with both signs of strain and the effect is more significant for compressive strain because the hole effective mass decreases with compressive strain but increases with tensile strain. The strain-induced suppression of interband and intraband scatterings plays also an important role in changing the hole mobility.

DOI: 10.1103/PhysRevB.78.245204 PACS number(s): 72.80.Cw, 71.20.Mq, 72.20.Fr

## I. INTRODUCTION

As silicon (Si) devices are rapidly approaching their physical and geometrical limits, various different solutions have been sought to overcome these limits, in order to maintain the downscaling trend articulated by Moore's law. There are two different approaches: one by strain engineering and material innovation (such as new materials for interconnect and gate) within the current paradigm of complementary metal-oxide-semiconductor (CMOS) technology and the other by different inventions beyond CMOS technology[1–4] such as molecular electronics and spintronics.[5,6] The key strategy by strain engineering is to use strain to increase the carrier mobility in Si.[1–4] It has been shown that tensile-strained Si ($\epsilon$-Si) grown on relaxed $Si_{1-x}Ge_x$ virtual substrates exhibits an electron mobility enhancement of 1.8–2.0 times.[7–9] The hole mobility in Si can be enhanced by a factor of 2 (Refs. 10 and 11) on the (001)/⟨110⟩ $p$-type metal-oxide-semiconductor field-effect transistors ($p$-MOSFETs) with 2 GPa uniaxial stress.

The importance of strain engineering in Si devices has also stimulated many theoretical studies.[12–23] However, our understanding of the strain effect on carrier mobility in Si is still far from complete. The theoretical calculation of carrier mobility requires the knowledge of accurate electronic band structures. Current methods of calculating band structures in strained systems include the $\mathbf{k}\cdot\mathbf{p}$ method,[13–18] tight-binding (TB),[19,20] empirical pseudopotential (EPM) (Ref. 21), and first-principles quantum mechanics[22,23] methods. The carrier mobilities are usually calculated by using the band structures obtained from the semiempirical methods, with good efficiency but poor accuracy. Recently, Dziekan *et al.*[23] attempted to combine more accurate first-principles band structures with Boltzmann transport equations to calculate the electron mobility in strained Si based on a constant relaxation-time approximation.

In this paper, we report calculations of both electron and hole mobility in biaxially strained Si by combining first-principles band-structure and Boltzmann transport theories without using the constant relaxation-time approximation. We take into account the change in relaxation time as a function of strain. We find that the assumption of constant relaxation time is a reasonably good approximation for calculating electron mobility in Si but a rather poor approximation for calculating hole mobility. This is because there is a large change in hole relaxation time due to the strain-induced suppression of interband and intraband scatterings. In general, tensile strain will increase both electron and hole mobilities; compressive strain will decrease electron mobility but will increase hole mobility. The carrier mobility is affected by the strain-induced change in electron and hole effective masses, while the hole mobility is also affected by the strain-induced suppression of interband and intraband scatterings.

## II. CALCULATION METHODS

We first carry out a systematic study of the band structures of bulk Si under biaxial strain, as indicated in Fig. 1(b), using first-principles methods based on density-functional theory. From the band structures, we calculate the effective masses of electrons and holes at the valence- and conduction-band edges and the band-splitting energies. Then we calculate the carrier mobility of electrons and holes as a function of strain using Boltzmann transport theory. For the calculation of Si band structures, we use a two-atom primitive cell. In applying the biaxial strain, the cell is strained equally in the $x$ and $y$ directions to the desired amount and allowed to relax fully in the $z$ direction [see Fig. 1(b)]. The atomic positions are relaxed and optimized until the forces on each atom become smaller than 0.001 eV/Å. We use projected augmented wave (PAW) potentials within the local-density approximation with a plane-wave cut-off energy of 400 eV, as implemented in the Vienna *ab initio* simulation package (VASP).[24] To consider the spin-orbit interaction, we perform relativistic calculations to get very accurate band structures. We use a $(10\times10\times10)$ mesh of $k$ points in the scheme of Monkhorst-Pack[25] for the Brillouin-zone sampling. The method for calculating effective mass and carrier mobility will be presented in Sec. III.

 

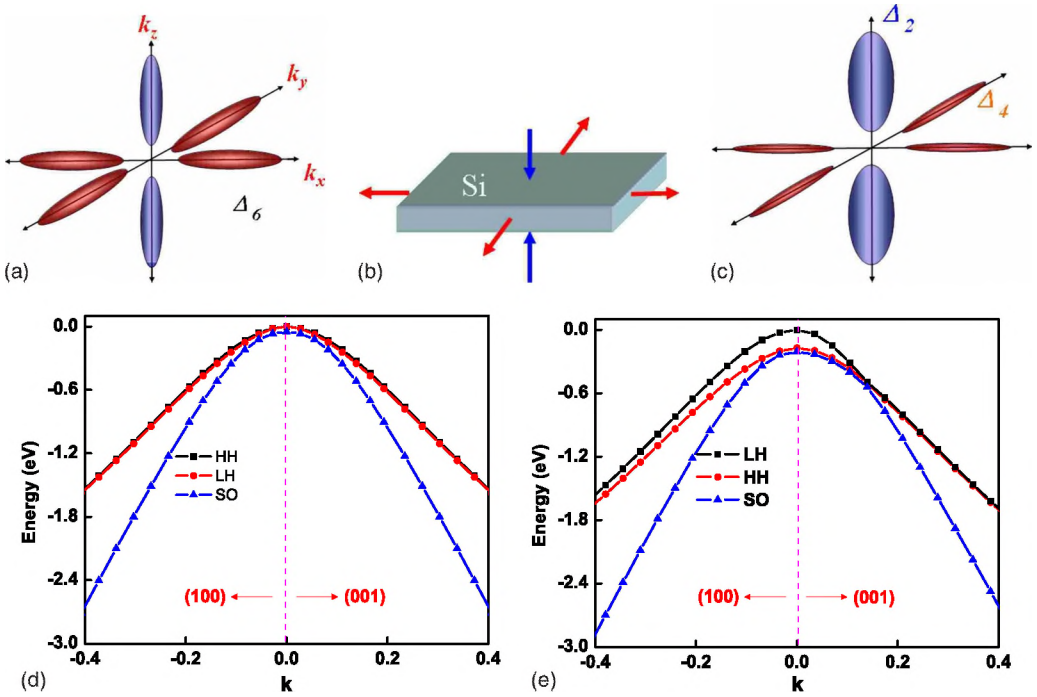


FIG. 1. (Color online) Si conduction- and valence-band structures as a function of biaxial strain. (a) The six Si conduction-band valleys along three different directions are equally populated without strain; (b) schematics of bulk Si under biaxial tensile strain; (c) under tensile strain, the valleys are split into two groups. Electrons tend to populate the lower $\Delta_2$ valleys than the higher $\Delta_4$ valleys; (d) and (e) show the three top valence bands near $\Gamma$ point for the strain-free and 1.5% biaxial tensile-strained Si, respectively.

## III. RESULTS AND DISCUSSION

In strain-free bulk silicon, the conduction-band minimum consists of six equivalent $\Delta_6$ valleys [Fig. 1(a)]. Under biaxial strain, the $\Delta_6$ valleys are split into two groups: four in-plane $\Delta_4$ valleys and two out-of-plane $\Delta_2$ valleys [Fig. 1(c)]. The top three valence bands of Si at the $\Gamma$ point are bands of heavy hole (HH), light hole (LH), and spin-orbit split-off (SO) hole, with HH and LH degenerate with each other and SO lying 44 meV below [Fig. 1(d)]. Under biaxial tensile or compressive strain, the valence bands become highly anisotropic and the crossover between bands happens [Fig. 1(e)]. Consequently, the designation of LH, HH, and SO bands loses its original meaning. To avoid confusion, we will always refer to the top three valence bands as LH, HH, and SO in the order of descending energy, respectively.

Figure 2 shows the Si conduction- and valence-band-edge energies as a function of applied biaxial strain. For conduction bands, the energy levels of both groups of $\Delta_2$ and $\Delta_4$ conduction-band valleys change linearly with strain, decreasing with tensile strain and increasing with compressive strain. Under tensile strain, the energy of the out-of-plane $\Delta_2$ valleys is lowered relative to that of the $\Delta_4$ in-plane valleys. The compressive strain, however, does the opposite. The energy splitting $\Delta E$ between these two groups of valleys is 162 meV per 1% tensile or compressive strain, in agreement with previous band-structure calculations.[26] For valence bands, strain induces a splitting between the LH and HH bands. Similar to the conduction bands, a tensile strain causes the energy levels of all three valence bands to decrease while a compressive strain increases their energy levels. Moreover, under tensile strain, the energy difference between HH and SO bands remains almost constant, while the energy difference between HH (or SO) and LH increases with the increasing strain. Under compressive strain, the energy difference between LH and HH is almost constant, while the difference between HH (or LH) and SO increases with strain.

The effective mass of electrons or holes is obtained using a parabolic band model at the bottom of conduction-band valleys or at the top of the valence bands by a parabolic fitting to the band dispersion of **E** vs **k** along different directions around the conduction-band minimum (electrons) or valence-band maximum (holes). The conduction-band valley has an ellipsoidal shape and the electron effective mass can be characterized by one longitudinal and two transverse

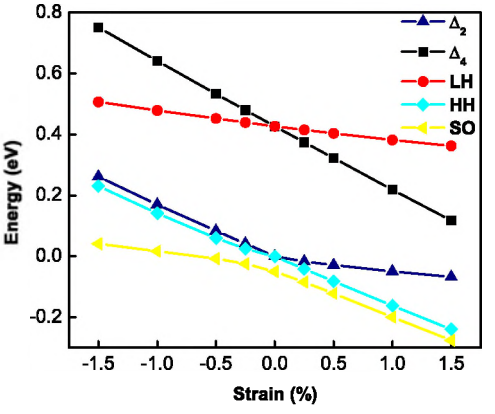


FIG. 2. (Color online) Change in Si conduction- and valence-band edges as a function of biaxial strain.

TABLE I. Effective masses for electrons ($e$), heavy holes (hh), light holes (lh), and spin-orbit split-off (so) holes (in units of the electron rest mass) for strain-free cubic Si.

| Ref. | $m_e$ | | $m_{\mathrm{hh}}^{(100)}$ | $m_{\mathrm{hh}}^{(110)}$ | $m_{\mathrm{hh}}^{(111)}$ | $m_{\mathrm{lh}}^{(100)}$ | $m_{\mathrm{lh}}^{(110)}$ | $m_{\mathrm{lh}}^{(111)}$ | $m_{\mathrm{so}}$ |
|---|---|---|---|---|---|---|---|---|---|
| This work | 0.95 ($m_l$) | 0.19 ($m_t$) | 0.22 | 0.36 | 0.66 | 0.22 | 0.17 | 0.13 | 0.22 |
| [a] | 0.96 ($m_l$) | 0.16 ($m_t$) | 0.26 | 0.54 | 0.67 | 0.18 | 0.14 | 0.13 | 0.22 |
| [b] | 0.92 ($m_l$) | 0.19 ($m_t$) | | | | | | | 0.23 |
| [c] | | | 0.46 | 0.53 | 0.56 | 0.17 | 0.16 | 0.16 | |
| [d] | | | 0.43 | 0.43 | 0.27 | 0.19 | 0.24 | | |

[a]Reference 22, first principles.
[b]Reference 27, experimental values.
[c]Reference 28, experimental values.
[d]Reference 29, experimental values.

masses. In Table I, we list the calculated effective masses of electrons and holes for bulk silicon in comparison with previous first-principles calculations and experiments. The spin-orbit split hole mass is isotropic in all **k** directions and is therefore listed as one value. In general, our results are in good agreement with the previous calculations.[22] In comparison to experimental results,[27–29] the general agreements are very good except that the heavy-hole masses along the (100) and (110) directions are underestimated by our calculations.

Under biaxial strain, the effective masses of both electrons and holes change noticeably. In the $\Delta_2$ valleys, we have two typical masses: the (001) longitudinal and the degenerate (100) and (010) transverse masses. In the $\Delta_4$ valleys, however, there are three typical masses: the degenerate (100) and (010) longitudinal, the degenerate (100) and (010) transverse, and the (001) transverse masses, in accordance with their respective symmetries along the in-plane or out-of-plane directions. In Fig. 3, we plot the longitudinal and transverse electron masses as a function of strain. It shows a linear relationship consistent with a recent first-principles study.[23] The electron effective mass varies less than 3% within the range of 1.5% applied strain.

Next, we calculate the electron effective mobility mass by considering contributions of the electron effective mass from each of the individual valleys as obtained above. The relative population of electrons in each valley is calculated as

$$n = 2\left(\frac{2\pi m_e^* k_B T}{h^2}\right)^{3/2} \exp\left(-\frac{E - E_f}{k_B T}\right), \tag{1}$$

where $m_e^* = \sqrt[3]{m^L m^{T1} m^{T2}}$ is called the electron-density-of-states mass, which is the mean effective mass averaged over effective mass along different directions. $m^L$, $m^{T1}$, and $m^{T2}$ are longitudinal and transverse masses in the valley. $k_B$ is the Boltzmann constant, $T$ is absolute temperature, $h$ is the Planck constant, $E$ is the minimum energy of each valley, and $E_f$ is the Fermi energy.

The in-plane effective mobility mass along the $x$ direction can then be calculated as

$$1/m_x^{\mathrm{eff}} = (n_{100}/m_{100}^{Lx} + n_{010}/m_{010}^{Tx} + n_{001}/m_{001}^{Tx})/(n_{100} + n_{010} + n_{001}), \tag{2}$$

where $n_{100}, n_{010}, n_{010}$ are the population of electrons in the (100), (010), and (001) valleys, respectively. $m_{100}^{Lx}$ is the longitudinal mass along the $x$ axis in the (100) valley, $m_{010}^{Tx}$ is the transverse mass along the $x$ axis in the (010) valley and $m_{001}^{Tx}$ is the transverse mass along the $x$ axis in the (001) valley. Due to the crystalline symmetry under strain, the (100) and (010) directions are equivalent so that the in-plane effective mass along the $y$ direction $m_y^{\mathrm{eff}}$ is equal to $m_x^{\mathrm{eff}}$, but the out-of-plane mass along $z$ direction $m_z^{\mathrm{eff}}$ is different. The effective electron mobility mass at 300 K is plotted in Fig. 4(a) as

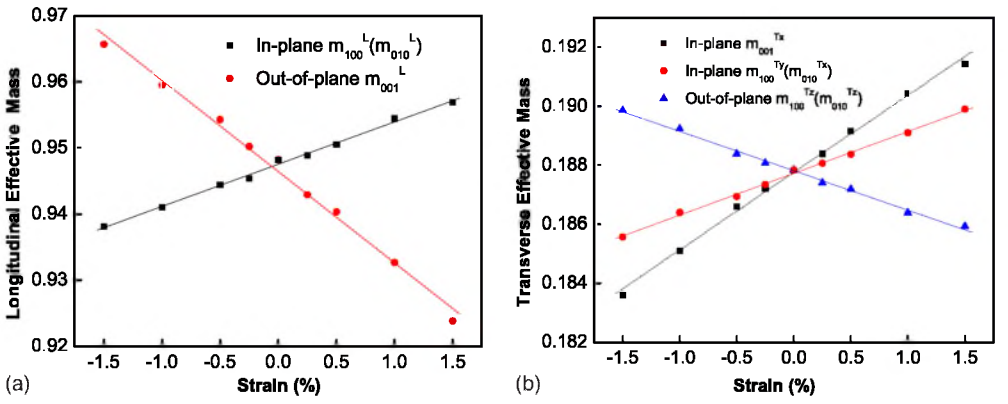


FIG. 3. (Color online) Electron effective mass as a function of biaxial strain. (a) The longitudinal mass. (b) The transverse mass.

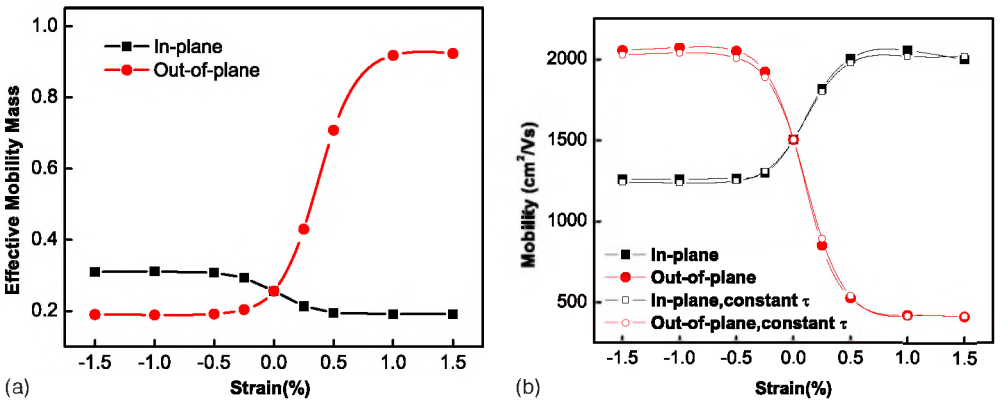


FIG. 4. (Color online) (a) Comparison of Si in-plane and out-of-plane electron effective mobility masses at 300 K as the function of biaxial strain. (b) Same as (a) for electron mobility obtained with (open symbols) and without (filled symbols) the constant relaxation-time approximation.

a function of strain. The in-plane mobility mass decreases with tensile strain and increases with compressive strain, while the out-of-plane mobility mass has the opposite behavior. We note that although strain induces a minimal change in the individual effective electron mass within each valley, we still see a rather large change in the overall effective mobility mass. This is because strain has greatly changed the relative population of electrons among two groups of different valleys.

Given the electron mobility mass ($m$) in a valley, we then calculate the electron mobility as

$$\mu = \frac{e\langle\tau\rangle}{m}, \tag{3}$$

where $e$ is the charge of electron, and $\tau$ is the relaxation time having contributions from both intravalley and intervalley phonon scatterings. For intravalley scattering, where only acoustic-phonon scattering involving a small change in wave vector is significant,[30] we have

$$\frac{1}{\tau_{\text{acoust}}(E)} = \frac{2\pi k_B T D_A^2}{\hbar \rho u_l^2} D(E). \tag{4}$$

The intervalley phonon-scattering rate (both $f$ and $g$ types) can be calculated by

$$\frac{1}{\tau_{\text{INV}}(E)} = \frac{\pi D_{if}^2 Z_f}{2\rho\omega_{if}}\left(N + \frac{1}{2} \pm \frac{1}{2}\right) D(E \mp \hbar\omega_{if} - \Delta E_{if}). \tag{5}$$

The average relaxation time is calculated as

$$\frac{1}{\tau(E)} = \frac{1}{\tau_{\text{acoust}(E)}} + \sum \frac{1}{\tau_{\text{INV}}(E)} \tag{6}$$

and

$$\langle\tau\rangle = \frac{\int_0^\infty \tau(E) E \times D(E) \times f(E) dE}{\int_0^\infty E \times D(E) \times f(E) dE}. \tag{7}$$

The density of states is calculated as

$$D(E) = \frac{\sqrt{2} m^{*3/2}}{\pi^2 \hbar^3} \sqrt{E}(1 + 5/2\alpha E). \tag{8}$$

In Eqs. (4)–(8), $D_A$ is the effective acoustic deformation potential, $\hbar$ is the reduced Planck constant, $\rho$ is the silicon density, $u_l$ is the longitudinal-acoustic velocity, $D_{if}$ is the intervalley effective deformation potential, $\hbar\omega_{if}$ is the intervalley phonon energy, $N$ is the Bose-Einstein distribution function, $f$ is the Fermi-Dirac distribution function, $Z_f$ is the number of available final states for the intervalley scattering, $m^*$ is the density-of-states mass, and $\alpha$ is the nonparabolicity parameter. The sum for the intervalley scattering rate in Eq. (6) accounts for both $g$ and $f$ types of scattering between valleys. Table II lists the values of all the parameters used in the calculation of relaxation time. Notice that in our calculations, we found that the effective acoustic deformation potential ($D_A$) value (9.9 eV) in the literature[12] is too large to reproduce the correct electron mobility in strain-free bulk Si, so we choose a smaller value of 7.8 eV.

In Fig. 4(b) we plot the electron mobility as a function of strain, as obtained by the weighted average over electron mobility in each valley. In strain-free Si, the electron mobility is calculated to be ~1500 $\text{cm}^2/\text{V s}$, in very good agreement with the experimental value.[31] The in-plane electron mobility can increase by up to 33% with a +0.5% tensile strain and decreases by as much as ~20% with a −0.5% compressive strain, but further increase in tensile or compressive strain beyond 0.5% will no longer affect the in-plane electron mobility. In contrast, the out-of-plane electron *mobility* decreases with tensile strain and increases with compressive strain. We can estimate the relative contribution to the change in electron mobility from the change in effective mobility mass or the suppression of phonon scattering. Figure 4(b) shows that the results obtained with or without the constant relaxation-time assumption are very close to each other, indicating that the electron relaxation time is not sensitive to strain. Since the relaxation time is determined by the phonon-scattering rate, these results also indicate that the suppression of intervalley phonon scattering due to the strain-induced band splitting (between the $\Delta_2$ and $\Delta_4$ bands) is not significant and the strain-induced reduction in effective

TABLE II. The parameters used in the carrier mobility calculations.

| | $D_A$ (eV) | $D_O$ ($10^8$ eV/cm) | $\hbar\omega_O$ (eV) | $\rho$ (g/cm$^3$) | $u_l$ ($10^5$ cm/s) | $\alpha$ (eV$^{-1}$) | $G_{ij}$ |
|---|---|---|---|---|---|---|---|
| Electron | 7.8 | | | 2.33[a] | 9.0[a] | 0.5[a] | |
| Hole | 7.12[b] | 13.24[b] | 0.0612[a] | 2.33[a] | 9.0[a] | 0.5[a] | 0.5[c] |
| Electron intervalley scattering | | | $D_{if}$[d] ($10^8$ eV/cm) | | | $\hbar\omega_{if}$[d] (eV) | |
| $g$ type | | | 0.5 | | | 0.012 (TA) | |
| | | | 0.8 | | | 0.019 (LA) | |
| | | | 11.0 | | | 0.061 (LO) | |
| $f$ type | | | 0.3 | | | 0.019 (TA) | |
| | | | 2.0 | | | 0.047 (LA) | |
| | | | 2.0 | | | 0.059 (LA) | |

[a]Reference 17, first principles.
[b]Reference 18, experimental values.
[c]Reference 13, experimental values.
[d]Reference 12, experimental values.

mobility mass must have played a dominant role.

Figure 5 shows the LH, HH, and SO hole effective masses as a function of strain. In contrast to the linear change in electron effective mass, the hole effective mass changes much more dramatically with strain. Because we are mostly interested in the mobility along the in-plane (100) or out-of-plane (001) direction, only the hole mass changes along those two directions are shown. In the (100) direction, the LH mass first increases quickly to about 10% when the tensile strain is increased to ~0.5% and then starts to decrease slightly with further increase in strain. When compressive strain is applied, the LH mass initially undergoes a quick drop and then increases slowly with further increase in strain. The HH mass drops sharply with the initial application of tensile strain and then decreases slowly with further increase in strain. Under compressive strain, the HH mass also increases sharply with the initial application of strain and then starts to decrease. The careful examination of the HH and LH mass changes with enough data points near the zero strain shows that their changes are continuous. At the start of either type of strain, one mass is pushed up and another mass is pushed down. The sharp change we see across zero strain in the figure is due to the band crossover, as shown in Fig. 1(e). The SO mass decreases with increasing tensile strain and increases with increasing compressive strain. The hole effective mass in the (001) direction shows an exactly opposite trend of change with strain in comparison to that in the (100) direction.

Using the same approach as for electron effective mobility mass, we have calculated the in-plane and out-of-plane effective hole mobility masses. Figure 6(a) shows that under tensile strain, the in-plane hole mobility mass first increases until strain is ~+0.5% and then starts to decrease. The initial increase is due to the band splitting which causes most of the holes to occupy the LH band with a heavier mass than they were in the HH and SO bands. As strain further increases, the hole mass in the LH band decreases and the overall effective mass starts to decrease. When compressive strain is applied, the in-plane effective hole mass decreases until reaching 90% of its strain-free value; the out-of-plane effective mass shows an opposite trend.

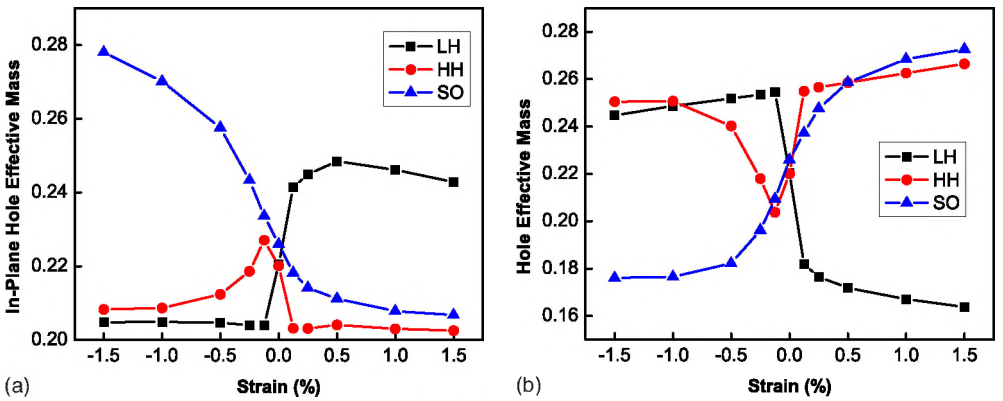


FIG. 5. (Color online) (a) In-plane hole effective mass as a function of biaxial strain. (b) Out-of-plane hole effective mass as a function of biaxial strain.

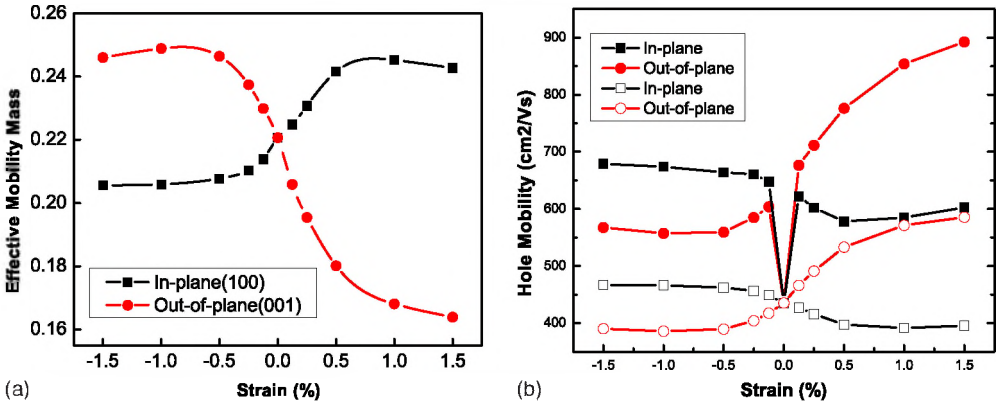


FIG. 6. (Color online) (a) The total hole effective mobility mass as a function of biaxial strain. (b) Same as (a) for hole mobility obtained with (open symbols) and without (filled symbols) the constant relaxation-time approximation.

For device applications, we are more concerned with hole mobility. It is generally agreed that the electron mobility will increase under tensile strain. Device fabrications would be simplified if hole mobility is also increased with tensile strain. However, so far the effect of biaxial tensile strain on hole mobility remains controversial. While some earlier experiments[32–34] report hole mobility enhancements with biaxial tensile strain, more recent reports[35–37] show that the hole mobility tends to decrease under tensile strain. On the other hand, the hole mobility seems always to increase under compressive strain.[3,4,36] Figure 6(b) shows our calculated hole mobility as a function of biaxial strain. The hole mobility calculations follow similar procedures as used for electron mobility calculations. In our calculations, we consider both intraband and interband acoustic- and optical-phonon scatterings. The scattering rate from $i$th to $j$th bands are calculated as

$$\frac{1}{\tau_{\text{acoust},ij}(E)} = \frac{2\pi k_B T D_A^2}{\hbar \rho u_l^2} D(E) G_{ij}, \tag{9}$$

$$\frac{1}{\tau_{\text{optical},ij}(E)} = \frac{\pi D_O^2}{\rho \omega_O}\left(N + \frac{1}{2} \pm \frac{1}{2}\right) D(E \mp \hbar\omega_O) G_{ij}. \tag{10}$$

Here, $G_{ij}$ is the overlap integral, $D_O$ is the effective optical deformation potential, and $\hbar\omega_O$ is the optical-phonon energy. The other parameters have the same meaning as that for electrons and the values for the parameters are listed in Table II.

Under strain-free conditions, the predicted hole mobility in bulk Si is about 434 $\text{cm}^2/\text{V s}$, in good agreement with the experimental value of $\sim$450 $\text{cm}^2/\text{V s}$.[38] Our calculations show that the hole mobility increases with both compressive and tensile strains, with a larger increase under compressive strain than under tensile strain. One previous theoretical calculation using the $\mathbf{k}\cdot\mathbf{p}$ method[17] also predicted the increase in hole mobility under both types of strain but instead showed a larger enhancement under tensile strain different from our results. This difference might be caused by a less accurate band structure used in their calculations.

Quantitatively, our calculations show that under tensile strain, the in-plane mobility [solid squares in Fig. 6(b)] first increases by $\sim$40% with a small strain of 0.125%. It then slightly decreases and increases again with further increase in strain, in correlation with the change in in-plane effective hole mass [Fig. 6(a)]. The out-of-plane mobility (solid circle) increases even more, steadily up to 200% at +1.5% of strain. Under compressive strain, the in-plane hole mobility first quickly jumps by $\sim$50% up to the point of −0.25% strain and then increases slowly with further increase in strain. The out-of-plane mobility increases less by $\sim$30% in the range of strain from −0.25% to −1.5%. The careful examination of enough data points also shows the mobility changes continuously as the strain approaches zero; it increases sharply to about 635 $\text{cm}^2/\text{V s}$ (by extrapolation) with the addition of either type of strain. This is due to the sharp change in effective mass as shown in Fig. 5.

In Fig. 6(b), we also plot the hole mobility change with strain obtained using the constant relaxation-time approximation (open squares and circles). By comparing the mobility enhancement with and without this approximation, it is clear that the hole mobility increase is mainly due to the suppression of interband and intraband scatterings. The larger increase in in-plane mobility at compressive strain is due to the decrease in effective mobility mass. The increase in effective mobility mass under tensile strain slightly cancels the effect of suppression of phonon scattering and results in a smaller increase in in-plane hole mobility. Our prediction is different from that calculated using the $\mathbf{k}\cdot\mathbf{p}$ method,[17] which predicts that hole mobility is more enhanced under a tensile strain. We note that our calculations also predict a hole mobility enhancement under tensile strain, in disagreement with some experimental results.[35–37] This disagreement may be attributed to the quantum confinement effect. In the experiments, within the narrow channel region, the strong quantum confinement effect[20] may already induce the band splitting under strain-free conditions and the interband and intraband scatterings are suppressed. With the addition of tensile strain, the contribution from suppression of phonon scattering becomes less significant and the increase in effective mobility mass becomes dominant. Therefore, the hole mobility may be lowered with a tensile strain.

Our calculation results can be used in the study of carrier mobility in strained nanostructures, such as Si/Ge nanotubes,[39] Si nanowires,[40] and Ge island-stressed Si

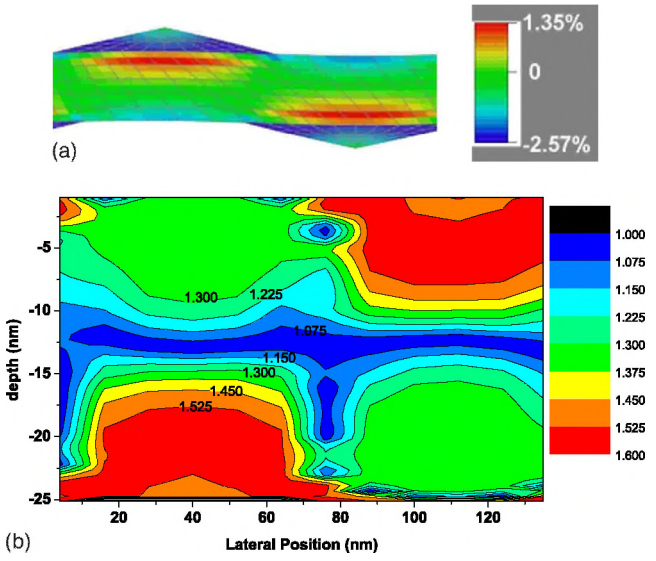


FIG. 7. (Color online) The hole mobility variation in a 25-nm-thick Si membrane strained by Ge islands (nanostressors) on both sides of the membrane. (a) Cross section of the strain distribution in the Si membrane and Ge islands and (b) cross-section modulation map of the hole mobility enhancement in the Si membrane.

membranes,[41] when quantum confinement effects are not significant.[42] Figure 7(a) shows a section of the Ge island-decorated Si membrane 25 nm thick. Due to the lattice mismatch between Ge and Si, a biaxial tensile strain is generated in Si membrane, which varies with location in the membrane. In Fig. 7(b), we plot the hole mobility enhancement distribution inside the Si membrane using the strain dependence of hole mobility obtained early in Fig. 6. The hole mobility changes periodically along the lateral direction due to the strain modulation induced by Ge islands acting as nanostressors. We envision that these kinds of study of carrier mobility change in strain-engineered nanostructures[43] will help in the rational design of new devices with specific functionality.

In conclusion, we have performed a systematic study of electronic properties of biaxially strained silicon and the effects of strain on charge carrier mobility using first-principles band-structure and Boltzmann transport theories. Our study shows that the electron mobility increases under tensile strain, which is mainly caused by the strain-induced decrease in electron effective mobility mass while the reduction in intervalley scattering plays a minor role. On the other hand, the hole mobility increases under both signs of strain, which is mainly caused by the reduction in phonon scattering. The increase in hole effective mobility mass with tensile strain leads to a smaller enhancement of hole mobility under tensile strain in comparison with that under compressive strain. Although our study of carrier mobility is carried out in strained bulk silicon, our results and approach will be generally useful for the prediction of carrier mobility in different strain-engineered nanostructures.

## ACKNOWLEDGMENT

This work was supported by the DOE (Grant No. DEFG0203ER46027). We thank M. G. Lagally and C. S. Ritz for sharing their experimental results of Ge island stressors on Si nanomembranes before publication as modeled in Fig. 7(a).

*dyu@eng.utah.edu
†fliu@eng.utah.edu

[1] J. R. Hwang *et al.*, *Performance of 70nm strained-silicon CMOS devices*, in Proceedings of Symposium on VLSI Technology Digest (Japan Society of Applied Physics, Tokyo, Japan, 2003), p. 103.
[2] Q. Xiang *et al.*, *Strained silicon NMOS with nickel-silicide metal gate*, in Proceedings of Symposium on VLSI Technology Digest (Japan Society of Applied Physics, Tokyo, Japan, 2003), p. 101.
[3] S. E. Thompson*et al.*, IEEE Trans. Electron Devices **51**, 1790 (2004).
[4] S. E. Thompson *et al.*, IEEE Electron Device Lett. **25**, 191 (2004).
[5] Q. Yan*et al.*, Nano Lett. **7**, 1469 (2007).
[6] D. Yu, E. M. Lupton, M. Liu, W. Liu, and F. Liu, J. Nanopart. Res. **1**, 56 (2008).
[7] J. Welser, J. L. Hoyt, and J. F. Gibbons, IEEE Electron Device Lett. **15**, 100 (1994).
[8] K. Rim, J. Welser, J. L. Hoyt, and J. F. Gibbons, *Enhanced hole mobilities in surface-channel strained-Si p-MOSFETS*, in Electron Devices Meeting, 10–13 Dec 1995 (IEEE, Washington, DC, USA, 1995), p. 517.
[9] M. T. Currie*et al.*, J. Vac. Sci. Technol. B **19**, 2268 (2001).
[10] L. Smith *et al.*, IEEE Electron Device Lett. **26**, 652 (2005).
[11] L. Washington, F. Nouri, S. Thirupapuliyur*et al.*, IEEE Electron Device Lett. **27**, 511 (2006).
[12] M. V. Fischetti and S. E. Laux, Phys. Rev. B **48**, 2244 (1993).
[13] S. K. Chun and K. L. Wang, IEEE Trans. Electron Devices **39**, 2153 (1992).
[14] E. X. Wang *et al.*, IEEE Trans. Electron Devices **53**, 1840 (2006).
[15] G. Y. Sun, Y. K. Sun, T. K. Nishida, and S. E. Thompson, J. Appl. Phys. **102**, 084501 (2007).
[16] D. Rideau, M. Feraille, L. Ciampolini, M. Minondo, C. Tavernier, H. Jaouen, and A. Ghetti, Phys. Rev. B **74**, 195208 (2006).
[17] M. V. Fischetti and S. E. Laux, J. Appl. Phys. **80**, 2234 (1996).
[18] M. V. Fischetti *et al.*, J. Appl. Phys. **94**, 1079 (2003).
[19] S. T. Chang, Jpn. J. Appl. Phys., Part 1 **45**, 3070 (2006).
[20] A. Khakifirooz and D. A. Antoniadis, IEEE Electron Device Lett. **27**, 402 (2006).
[21] J. R. Chelikowsky and M. L. Cohen, Phys. Rev. B **14**, 556 (1976).
[22] L. E. Ramos, L. K. Teles, L. M. R. Scolfaro, J. L. P. Castineira, A. L. Rosa, and J. R. Leite, Phys. Rev. B **63**, 165210 (2001).
[23] T. Dziekan, P. Zahn, V. Meded, and S. Mirbt, Phys. Rev. B **75**,

195213 (2007).
[24] G. Kresse and J. Furthmuller, *VASP the Guide* (Vienna University of Technology, Vienna, 2001).
[25] H. J. Monkhorst and J. D. Pack, Phys. Rev. B **13**, 5188 (1976).
[26] Th. Vogelsang and K. R. Hofmann, Appl. Phys. Lett. **63**, 186 (1993).
[27] G. Harbeke, O. Madelugn, and U. Rössler, in *Numerical Data and Functional Relationships in Science and Technology*, edited by O. Madelung (Springer-Verlag, Berlin, 1982), Vol. 17.
[28] R. N. Dexter and B. Lax, Phys. Rev. **96**, 223 (1954).
[29] R. N. Dexter, H. J. Zeiger, and B. Lax, Phys. Rev. **104**, 637 (1956).
[30] S. Takagi, J. L. Hoyt, J. Welser, and J. F. Gibbons, J. Appl. Phys. **80**, 1567 (1996).
[31] F. Schäffler, H.-J. Herzog, H. Jorke, and E. Kasper, J. Vac. Sci. Technol. B **9**, 2039 (1991).
[32] T. Mizuno, N. Sugiyama, A. Kurobe, and S. Takagi, IEEE Trans. Electron Devices **48**, 1612 (2001).
[33] C. W. Leitz, M. T. Currie, M. L. Lee, Z. Y. Cheng *et al.*, J. Appl. Phys. **92**, 3745 (2002).
[34] L. Huang *et al.*, IEEE Trans. Electron Devices **49**, 1566 (2002).
[35] H. Irie, K. Kita, K. Kyuno, and A. Toriumi, *In-plane mobility anisotropy and universality under uniaxial strains in n- and p-MOS inversion layers on (100), [110], and (111) Si*, in Electron Devices Meeting, 13–15 Dec 2004, IEDM Technical Digest (IEEE, San Francisco, CA, 2004), p. 225.
[36] K. Uchida, R. Zednik, C.-H. Lu, H. Jagannathan *et al.*, *Experimental study of biaxial and uniaxial strain effects on carrier mobility in bulk and ultrathin-body SOI MOSFETS*, in Electron Devices Meeting, 13–15 Dec 2004, IEDM Technical Digest (IEEE, San Francisco, CA, 2004), p. 229.
[37] P. C. Kuo, A. Jamshidi-Roudbari, and M. Hatalis, Appl. Phys. Lett. **91**, 243507 (2007).
[38] R. A. Logan and A. J. Peters, J. Appl. Phys. **31**, 122 (1960).
[39] J. Zang, M. H. Huang, and F. Liu, Phys. Rev. Lett. **98**, 146102 (2007).
[40] S. C. Rustagi *et al.*, IEEE Electron Device Lett. **28**, 909 (2007).
[41] M. H. Huang *et al.* (unpublished).
[42] F. Liu, P. Rugheimer, E. Mateeva, D. E. Savage, and M. G. Lagally, Nature (London) **416**, 498 (2002).
[43] M. Huang *et al.*, Adv. Mater. (Weinheim, Ger.) **17**, 2860 (2005).